

Possible X-ray diagnostic for jet/disk dominance in Type 1 AGN

Barbara J. Mattson*, Kimberly A. Weaver

NASA/Goddard Space Flight Center, Astrophysics Science Division, Greenbelt, MD, 20771

and

Christopher S. Reynolds

Department of Astronomy, University of Maryland, College Park, MD, 20742

ABSTRACT

Using *Rossi X-ray Timing Explorer* Seyfert 1 and 1.2 data spanning 9 years, we study correlations between X-ray spectral features. The sample consists of 350 time-resolved spectra from 12 Seyfert 1 and 1.2 galaxies. Each spectrum is fitted to a model with an intrinsic powerlaw X-ray spectrum produced close to the central black hole that is reprocessed and absorbed by material around the black hole. To test the robustness of our results, we performed Monte Carlo simulations of the spectral sample. We find a complex relationship between the iron line equivalent width (EW) and the underlying power law index (Γ). The data reveal a correlation between Γ and EW which turns over at $\Gamma \lesssim 2$, but finds a weak anti-correlation for steeper photon indices. We propose that this relationship is driven by dilution of a disk spectrum (which includes the narrow iron line) by a beamed jet component and, hence, could be used as a diagnostic of jet-dominance. In addition, our sample shows a strong correlation between R and Γ , but we find that it is likely the result of modeling degeneracies. We also see the X-ray Baldwin effect (an anti-correlation between the 2-10 keV X-ray luminosity and EW) for the sample as a whole, but not for the individual galaxies and galaxy types.

Subject headings: galaxies: Seyfert, X-rays: galaxies

*also Department of Astronomy, University of Maryland, College Park, MD and Adnet Systems, Inc., Rockville, MD

1. Introduction

Time-resolved X-ray spectroscopy studies of active galactic nuclei (AGN) offer the opportunity to investigate emission regions near the central black hole. In fact, X-ray spectroscopy offers the clearest view of processes occurring very close to the black hole itself, probing matter to its final plunge into the black hole. Armed with such information, we can unlock the structure of the innermost regions of AGN.

Typical X-ray spectra of AGN show an underlying powerlaw produced near the central black hole with signatures of reprocessed photons often present. These reprocessed photons show up as an Fe $K\alpha$ line at ~ 6.4 keV and a “reflection hump” which starts to dominate near 10 keV and is produced by the combined effects of photoelectric absorption and Compton downscattering in optically-thin cold matter irradiated by the hard X-ray continuum. The Fe $K\alpha$ line has been observed in both type 1 (unabsorbed) and type 2 (absorbed) Seyfert galaxies. It has been attributed to either the broad line region, the accretion disk, the molecular torus of unification models (Antonucci 1993), or some combination of these. Signatures of reflection have also been observed in both Seyfert 1 and 2 galaxies.

If the unification models are correct, we should see similar spectral correlations between Seyfert 1 and 2 galaxies, with any differences easily attributable to our viewing angle. Regardless of the accuracy of the reflection models, we expect changes in the underlying continuum to drive changes in the reprocessing features. However, results from X-ray spectral studies of AGN have so far produced puzzling results. Samples of Seyfert 1 observations from *ASCA* (Weaver, Gelbord & Yaqoob 2001) and *Rossi X-ray Timing Explorer* (Markowitz, Edelson, & Vaughan 2003) have shown no obvious relationship between changes in the continuum and iron line. Several galaxies have shown an anticorrelation between reflection and/or iron line equivalent width and the source flux; e.g. NGC 5548 (Chiang et al. 2000), MCG –6-30-15 (Papadakis et al. 2002), NGC 4051 (Papadakis et al. 2002; Wang et al. 1999), NGC 5506 (Papadakis et al. 2002; Lamer, Uttley & McHardy 2000). Recent data from *Suzaku* on MCG –6-30-15, on the other hand, show that the iron line and reflection remain relatively constant while the powerlaw is highly variable (Miniutti et al. 2006). Zdziarski, Lubiński & Smith (1999) found that Seyfert galaxies and X-ray binaries show a correlation between the continuum slope and reflection fraction, so those with soft intrinsic spectra show stronger reflection than those with hard spectra. However, other studies have found either a shallower relationship than Zdziarski et al. (Perola et al. 2002) or an anticorrelation (Papadakis et al. 2002; Lamer, Uttley & McHardy 2000).

Here we present the first results of a larger study of the X-ray spectral properties of Seyfert galaxies observed by the *Rossi X-ray Timing Explorer* (*RXTE*). Our full study consists of observations of 30 galaxies. In this letter, we focus on the spectral results from

the subset of 12 Seyfert 1 and 1.2 galaxies. In § 2 we present our method of data analysis, including our sample selection criteria (§ 2.1), a description of our data pipeline (§ 2.2), and results of our spectral analysis (§ 2.3). We discuss the implications of our results in § 3 and detail our conclusions in § 4.

2. Data Analysis

2.1. The Sample

The *RXTE* public archive¹ represents one of the largest collections of X-ray data for AGN, with pointed observations of over 100 AGN spanning 10 years. The *RXTE* bandpass allows the study of absorption and iron line properties of AGN spectra, as well as a glimpse at the Compton reflection hump. We use data from the *RXTE* proportional counter array (PCA), which is sensitive to energies from 2 to 60 keV and consists of five Proportional Counter Units (PCUs). Most of the sources in our sample do not show significant counts in the *RXTE* Hard Energy X-ray Timing Experiment (HEXTE), so we do not include HEXTE data in this study.

To focus this study, we choose only Seyfert galaxies for which the *RXTE* public archive contained a minimum of two pointings separated by at least two weeks. We further required the total observed time be > 40 ks. These selection criteria led to a sample of 40 Seyfert galaxies. For the analysis presented here, we examine the 18 Seyfert 1 and 1.2 galaxies. Six galaxies were eliminated after they were put through our data pipeline (see § 2.2 for more), so the final sample presented here consists of 12 galaxies, listed in Table 1. Because the data come from the public archive, the sample is not uniform from galaxy to galaxy or even from observation to observation; however, we use the Standard 2 data, which provides a standard data mode for these diverse observations.

2.2. Data Pipeline

To ensure consistent data reduction of the large volume of data, we developed a data pipeline. The Standard 2 data for each observation was reduced using a combination of FTOOLS and the Python[®] scripting language. The pipeline produces time-resolved spectra,

¹Hosted by the High Energy Astrophysics Science Archive and Research Center (HEASARC; <http://heasarc.gsfc.nasa.gov/>)

each with a minimum of 125,000 net photons, which are extracted using standard PCA selection criteria and background models (Jahoda et al. 2006). Sources which did not have sufficient net photons for even one spectrum were eliminated from the final sample (Table 1 shows the final sample with the 6 eliminated sources listed in the table notes). Each spectrum includes 1% systematic errors. We are confident in the instrument response and background models up to energies of ~ 25 keV, so we ignore channels with higher energies.

2.3. Spectral Fitting and Results

The data pipeline produced 350 spectra for the 12 galaxies in our sample. Each spectrum was fitted from 3 to 25 keV with an absorbed Compton reflection model plus a Gaussian iron line. In `xspec`, the PEXRAV (Magdziarz & Zdziarski 1995) model simulates the effects of an exponentially cut-off powerlaw reflected by neutral matter and has seven model parameters: photon index of the intrinsic underlying power-law (Γ), the cutoff energy of the power law in keV (E_c), the relative amount of reflection (R), the redshift (z), the abundance of heavy elements in solar units (Z), the disk inclination angle (i), and the photon flux of the power law at 1 keV in the observer’s frame (A). The relative amount of reflection is normalized to 1 for the case of an isotropic source above a disk of neutral material ($\Omega = 2\pi$). Adding a Gaussian line (energy in keV (E_{Fe}), physical width (σ) in keV, and normalization in units of photons $\text{cm}^{-2} \text{s}^{-1}$) and an absorbing column (N_H , in cm^{-2}) yields a total of 12 parameters.

We fixed the following values in PEXRAV: $E_c = 500$ keV, $Z = 1.0$, and $\cos i = 0.95$. This inclination represents an almost face-on disk; however, since we are seeking trends in the spectral parameters, rather than absolute values, the precise value is not important to this study. In addition, z is fixed at the appropriate value from the NASA Extragalactic Database for each galaxy². After fitting all spectra to this model, we derived the mean Gaussian width for each source (Table 1), then held σ fixed for a second fit to the model. Our final model has free parameters: Γ , R , A , E_{Fe} , iron line normalization and N_H . To prevent `xspec` from pursuing unphysical values of the parameters, we set the following hard limits: $0 \leq \Gamma \leq 5$, $0 \leq R \leq 5$, $5.5 \leq E_{Fe} \leq 7.5$ keV, and $0 \leq \sigma \leq 1.5$ keV (for the free- σ fits).

Looking at the iron line equivalent width (EW) and Γ , we find a complex relationship with a “hump” peaking near $\Gamma \sim 2.0$ (Figure 1a). The EW - Γ plot shows a correlation for $\Gamma \lesssim 2.0$ and an anti-correlation for $\Gamma \gtrsim 2.0$, with a peak near $\Gamma \sim 2.0$ with $EW \sim 250$ eV. We also find a strong correlation between R and Γ (Figure 2a), with a best-fit line of

²<http://nedwww.ipac.caltech.edu/>

$$R = -0.87 + 0.54 \Gamma \quad (\chi^2 = 506/349 = 1.46).$$

We performed a Monte Carlo simulation to determine if our results were an artifact of modeling degeneracies. Each spectrum in the Monte Carlo sample was simulated with $N_H=10^{22} \text{ cm}^{-2}$, $\Gamma=2.0$, $R=1.0$, $E_{Fe}=6.4 \text{ keV}$, and $\sigma_{Fe}=0.23 \text{ keV}$. The flux and exposure times were randomly varied for each spectrum. The flux was varied by randomly choosing A from a uniform distribution between 0.004 and 0.06 photons $\text{keV}^{-1} \text{ cm}^{-2} \text{ s}^{-1}$. The exposure time was randomly generated from a uniform distribution between 300 and 11000s. The ranges for A and the exposure time represent the range of A and exposure for the spectra in the full sample.

We generated 200 spectra: 100 simulated using an *RXTE* Epoch 3 response, 50 using an Epoch 4 response, and 50 using an Epoch 5 response, roughly corresponding to our *RXTE* sample. Each spectrum was then fitted to the same model as our full sample. The R over Γ plot (Figure 2b) clearly shows a strong correlation with a best-fit line of $R = -7.3 + 4.1 \Gamma$ ($\chi^2 = 28.96/159 = 0.182$), which strongly suggests that the observed R - Γ correlation is a result of modeling degeneracies. The correlation shows a much steeper relationship than the Seyfert 1 data, due to the large number of Seyfert 1 spectra showing $R \sim 0$.

EW and Γ , however, do not suffer the same degeneracies, which is clear from the Monte Carlo results (Figure 1b). Based on the lack of correlation in our Monte Carlo results, we are confident that the shape of the EW - Γ plot for the data sample is real.

To further examine the EW - Γ relationship, we reproduced the EW - Γ plot to show the contribution from each galaxy (Figure 3). The radio-loud galaxies form the rising leg, with the quasar, 3C 273, anchoring the low Γ -low EW portion of the plot. The Seyfert 1 (radio quiet) and 1.2 galaxies tend to congregate at the peak and the falling leg of the plot. The one narrow-line Seyfert 1 diverges from the main cluster of points.

Finally, we examined EW as a function of the intrinsic 2-10 keV X-ray luminosity (L_x), using $H_0 = 70 \text{ km s}^{-1} \text{ Mpc}^{-1}$. We fitted the data for each galaxy, each type, and the sample as a whole to linear and powerlaw models. The data were well-fit for either model. For consistency with other publications, we report here the powerlaw results. For the sample as a whole, we see an anticorrelation, i.e. the X-ray Baldwin effect (Iwasawa & Taniguchi 1993), with $EW \propto L_x^{-0.14 \pm 0.01}$. When examining galaxy types, however, the anticorrelation does not always hold up (Table 1). We find an anticorrelation in the radio loud galaxies and the Seyfert 1.2s, but a marginal correlation for the quasar and radio quiet Seyfert 1s.

3. Discussion

3.1. EW - Γ Relationship

The simulations of George & Fabian (1991) for the observed spectrum from an X-ray source illuminating a half-slab showed that the spectra should include a “Compton hump” and an iron line. They found that the iron line EW should decrease as the spectrum softens. This is easy to understand, since as the spectrum softens (Γ increases), there are fewer photons with energies above the iron photoionization threshold. Our results show that the relationship between EW and Γ is not quite so simple. We find a correlation between EW and Γ when $\Gamma \lesssim 2$ and an anticorrelation when $\Gamma \gtrsim 2$. Other researchers have found a correlation for Seyfert 1 samples (Perola et al. 2002; Lubiński & Zdziarski 2001), but the galaxies in their samples primarily fell in the $\Gamma \lesssim 2$ region. Page et al. (2004) also find that their data suggest a slight correlation for a sample of radio loud and radio quiet Type 1 AGN.

A close examination of our EW - Γ plot shows that the data for different galaxy types progresses across the plot. The plot is anchored at the low- Γ , low- EW end by the quasar, 3C 273, in our sample. The rising arm of the plot, $\Gamma \sim 1.5 - 2.0$ and $EW \sim 0 - 300$ eV, is primarily formed by radio loud Seyfert 1 galaxies. The radio-quiet Seyfert 1 galaxies cluster near the $\Gamma \sim 2.0$, $EW \sim 300$ eV peak of the hump, and the radio-quiet Seyfert 1.2 galaxies form the falling arm of the plot for $\Gamma > 2.0$.

Physically, the most obvious difference between these sources is the presence or absence of a strong jet. We propose that this relationship is driven by the degree of jet-dominance of the source. The iron line features are associated with the X-ray emission from the disk. Since the disk is essentially isotropic, it will excite an observable iron line from matter out of our line-of-sight. On the other hand, the jet is beamed away from the obvious configurations of matter in the system and, more importantly, is beamed toward us in the quasar and radio-loud sources. Both of these jet-related phenomena reduce the observed equivalent width of any iron line emission associated with the jet continuum.

In order for the Γ to increase as the jet-dominance decreases, the jet in these sources must have a hard X-ray component, which implies that the radio-loud Seyferts in our sample are to be associated with low-peaked BL Lac objects (LBLs). BL Lac objects show two broad peaks in their spectral energy density plots (Giommi & Padovani 1994), with the lower-energy peak due to synchrotron emission and the higher-energy peak due to inverse Compton emission. BL Lacs are divided into two classes, depending on where the peaks occur: high-peaked BL Lacs (HBLs) and LBLs. The X-ray continuum in the HBLs is rather soft, since we are seeing the synchrotron spectrum cutting off in these sources. LBLs, on the other hand, tend to

have a harder X-ray continua, since we are observing well into the inverse Compton part of the spectrum (Donato, Sambruna, & Gliozzi 2005).

We also note that much of the falling arm of the EW - Γ relationship is formed by MCG –6-30-15. Recent observations of MCG –6-30-15 by Suzaku have shown that the reflection component, including the iron line, remains relatively constant Miniutti et al. (2006). We would expect, then, that as Γ increases, the EW should decrease, which is exactly what we see in our data.

3.2. R - Γ Relationship

Significant degeneracies between the photon index, absorbing column, and reflection fraction can easily lead to false conclusions about spectral correlations. These degeneracies occur as these three parameters trade off against each other in the modeling process, an effect that is especially strong in the $RXTE$ bandpass. Our R - Γ plot shows a strong correlation which is mimicked in our Monte Carlo results. The few points that lie under the main concentration are likely to be outliers, and not indicative of a subclass of galaxy. These points all come from spectra that have been fitted to have $N_H = 0$, and are primarily radio-loud galaxies. We conclude that the observed R - Γ correlation in our sample cannot be trusted as a real correlation.

3.3. EW - L_x Relationship

Looking at the EW - L_x relationship, we do see the X-ray Baldwin effect for our sample as a whole, with a slightly shallower anticorrelation than reported elsewhere. We find $EW \propto L_x^{-0.14}$, whereas Iwasawa & Taniguchi (1993) and Jiang, Wang & Wang (2006) find $EW \propto L_x^{-0.20}$ and Page et al. (2004) find $EW \propto L_x^{-0.17}$. However, when Jiang, Wang & Wang (2006) exclude the radio loud galaxies from their sample, they find $EW \propto L_x^{-0.10}$.

We find, though, that when we examine our data on a galaxy-by-galaxy or type-by-type basis, the effect is not consistent from source to source. At this point, we cannot determine if these variations are real or are simply due to the small number of spectra for some of our galaxies and types.

4. Conclusions

We have examined time-resolved spectra of 12 Seyfert 1 and 1.2 galaxies observed by *RXTE* over seven years. We find a complex relationship between the iron line equivalent width and the continuum slope, with a correlation for $\Gamma \lesssim 2$ that turns over to an anticorrelation for $\Gamma \gtrsim 2$. We propose that this relationship is a possible diagnostic for jet- versus disk-dominated sources, where jet-dominated sources show a correlation between EW and Γ , and disk-dominated sources show an anticorrelation. We also see a strong correlation between Γ and R which is likely an artifact of modeling degeneracies caused by the interplay of Γ , R , and n_H in the *RXTE* bandpass. Finally, we observe the X-ray Baldwin effect for the sample as a whole, but not for each galaxy and galaxy type individually.

This research has made use of data obtained from the High Energy Astrophysics Science Archive Research Center (HEASARC), provided by NASA’s Goddard Space Flight Center.

This research has also made use of the NASA/IPAC Extragalactic Database (NED) which is operated by the Jet Propulsion Laboratory, California Institute of Technology, under contract with the National Aeronautics and Space Administration.

CSR gratefully acknowledges support from the National Science Foundation under grants AST0205990 and AST0607428.

REFERENCES

- Antonucci, R. 1993, *ARA&A*, 31, 473
- Chiang, J. 2000, *ApJ*, 528, 292
- Donato, D., Sambruna, R. M., Gliozzi, M. 2005, *Å*, 433, 1163
- George, I. M., Fabian, A. C. 1991, *MNRAS*, 249, 352
- Giommi, P., Padovani, P. 1994, *MNRAS*, 268, 51
- Iwasawa, K. Taniguchi, Y. 1993, *ApJ*, 413, L15
- Jahoda, K., Markwardt, C. B., Radeva, Y., Rots, A. H., Stark, M. J., Swank, J. H., Strohmayer, T. E., Zhang, W., 2006, *ApJS*, 163, 401
- Jiang, P., Wang, J. X., Wang, T. G. 2006, *ApJ*, 644, 725

- Lamer, G., Uttley, P., McHardy, I. M. 2000, MNRAS, 319, 949
- Lubiński, P., Zdziarski, A. A. 2001, MNRAS, 323, L37
- Magdziarz, P. & Zdziarski, A. A. 1995, MNRAS, 273, 837
- Markowitz, A., Edelson, R., Vaughan, S. 2003, ApJ, 598, 935
- Miniutti, et al. 2006, PASJ, accepted (astro-ph/0609521)
- Page, K. L., O'Brien, P. T., Reeves, J. N. Turner, M. J. L. 2004, MNRAS, 347, 316
- Papadakis, I. E., Petrucci, P. O., Maraschi, L., McHardy, I. M., Uttley, P., Haardt, F. 2002, ApJ, 573, 92
- Perola, G. C., Matt, G., Cappi, M., Fiore, G., Guainazzi, M., Maraschi, L., Petrucci, P. O., Piro, L. 2002, A&A, 389, 802
- Wang, J. X., Zhou, Y. Y., Xu, H. G., Wang, T. G. 1999, ApJ, 516, L65
- Weaver, K. A., Gelbord, J., Yaqoob, T. 2001, ApJ, 550, 261
- Zdziarski, A. A., Lubiński, P., Smith, D. A. 1999, MNRAS, 303, L11

Table 1. Sample of *RXTE*-observed Seyfert 1 and 1.2 galaxies^a

Galaxy	Seyfert Type ^b	Fitted Spectra ^c	Average $\sigma_{FeK\alpha}$ ^d	EW/L_x correlation ^e	
				α	WV/Num.
All				$-0.14^{+0.01}_{-0.01}$	700/350
Quasars				$+0.09^{+0.20}_{-0.25}$	105/81
3C 273	1	81	0.329	$+0.09^{+0.20}_{-0.25}$	105/81
Broadline Seyfert 1s				$-0.24^{+0.14}_{-0.15}$	48.0/66
3C 111	1	4	0.239	$+0.70^{+2.60}_{-1.52}$	0.654/4
3C 120 ^f	1	40	0.261	$-0.70^{+0.63}_{-0.61}$	20.9/39
3C 382	1	5	0.328	$-0.80^{+1.69}_{-1.70}$	2.54/5
3C 390.3	1	17	0.203	$-0.51^{+0.44}_{-0.41}$	2.70/17
Seyfert 1s (Radio quiet)				$0.01^{+0.30}_{0.30}$	23.6/31
Ark 120	1	15	0.197	$-0.66^{+0.58}_{-0.57}$	6.62/15
Fairall 9	1	16	0.155	$+0.41^{+0.44}_{-0.44}$	11.1/16
Seyfert 1.2s				$-0.08^{+0.03}_{-0.03}$	192/169
IC 4329A	1.2	41	0.214	$-0.55^{+0.36}_{-0.37}$	27.5/41
MCG -6-30-15	1.2	75	0.292	$-0.65^{+0.34}_{-0.33}$	89.2/75
Mkn 509	1.2	16	0.102	$-0.52^{+0.91}_{-0.99}$	7.57/16
NGC 7469	1.2	37	0.145	$-0.58^{+0.30}_{-0.31}$	17.7/37
Narrow Line Seyfert 1				$8.80^{+20.80}_{-6.08}$	0.196/3
TON S180	1.2	3	0.379	$8.80^{+20.80}_{-6.08}$	0.196/3

^aThe following sources were eliminated after running the data pipeline described in the text, due to having no spectra with at least 125,000 net photons: Mkn 110, PG 0804+761, PG 1211+143, Mkn 79, Mkn 335, and PG 0052+251.

^bSeyfert type based on the NASA Extragalactic Database

^cTotal number of spectra extracted using our data pipeline (§ 2.2).

^dThe average physical width of the Fe K α line for all spectra from a source when fitted to the absorbed powerlaw model with Compton reflection and Gaussian iron line (§ 2.3).

^eResults of fitting the X-ray luminosity over EW plot to a powerlaw model; e.g. $EW \propto L_x^\alpha$, where L_x is the 2-10 keV X-ray luminosity in ergs s⁻¹ and EW is the iron line equivalent width in eV.

^fOne 3C 120 spectrum shows a flare, where L_x jumps by $\sim 6\times$. The number quoted above excludes this point from the sample. If we include the flare, we find $EW \propto L_x^{0.07(+0.18/-0.25)}$.

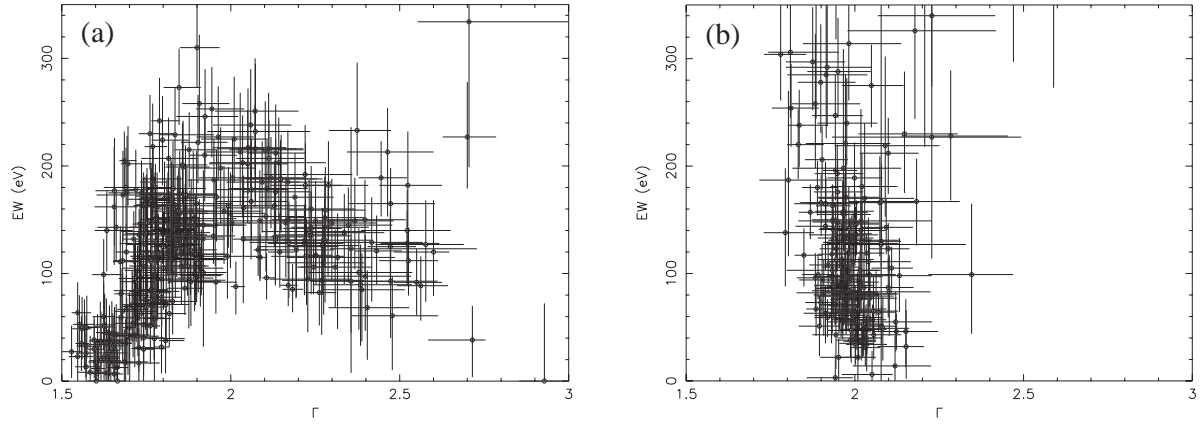


Fig. 1.— Iron line equivalent width in eV (EW) versus powerlaw photon index (Γ) for the Seyfert 1/1.2 sample (a) and for the Monte Carlo simulations (b).

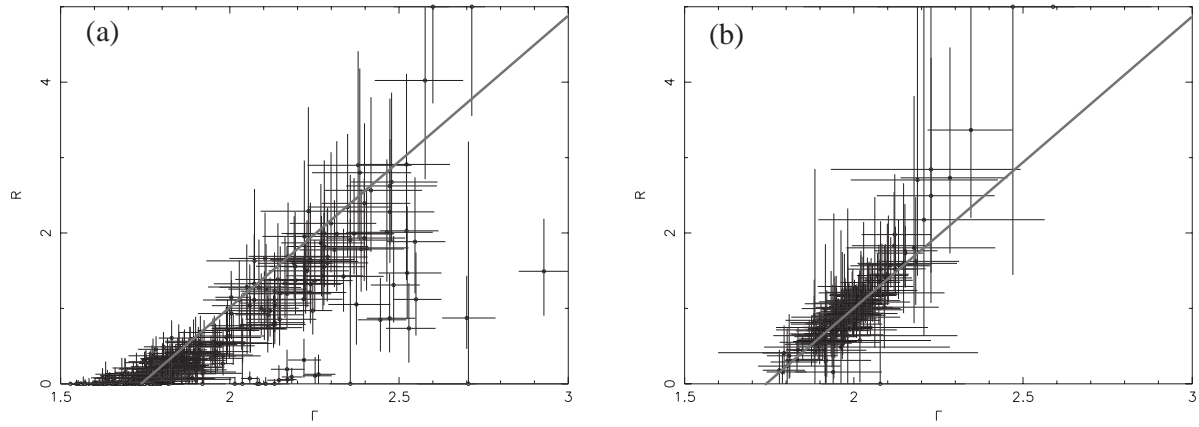


Fig. 2.— Reflection fraction (R) versus powerlaw photon index (Γ) for the Seyfert 1/1.2 sample (a) and for the Monte Carlo simulations (b). In both plots, the line shows the best-fit linear model for the Monte Carlo simulations.

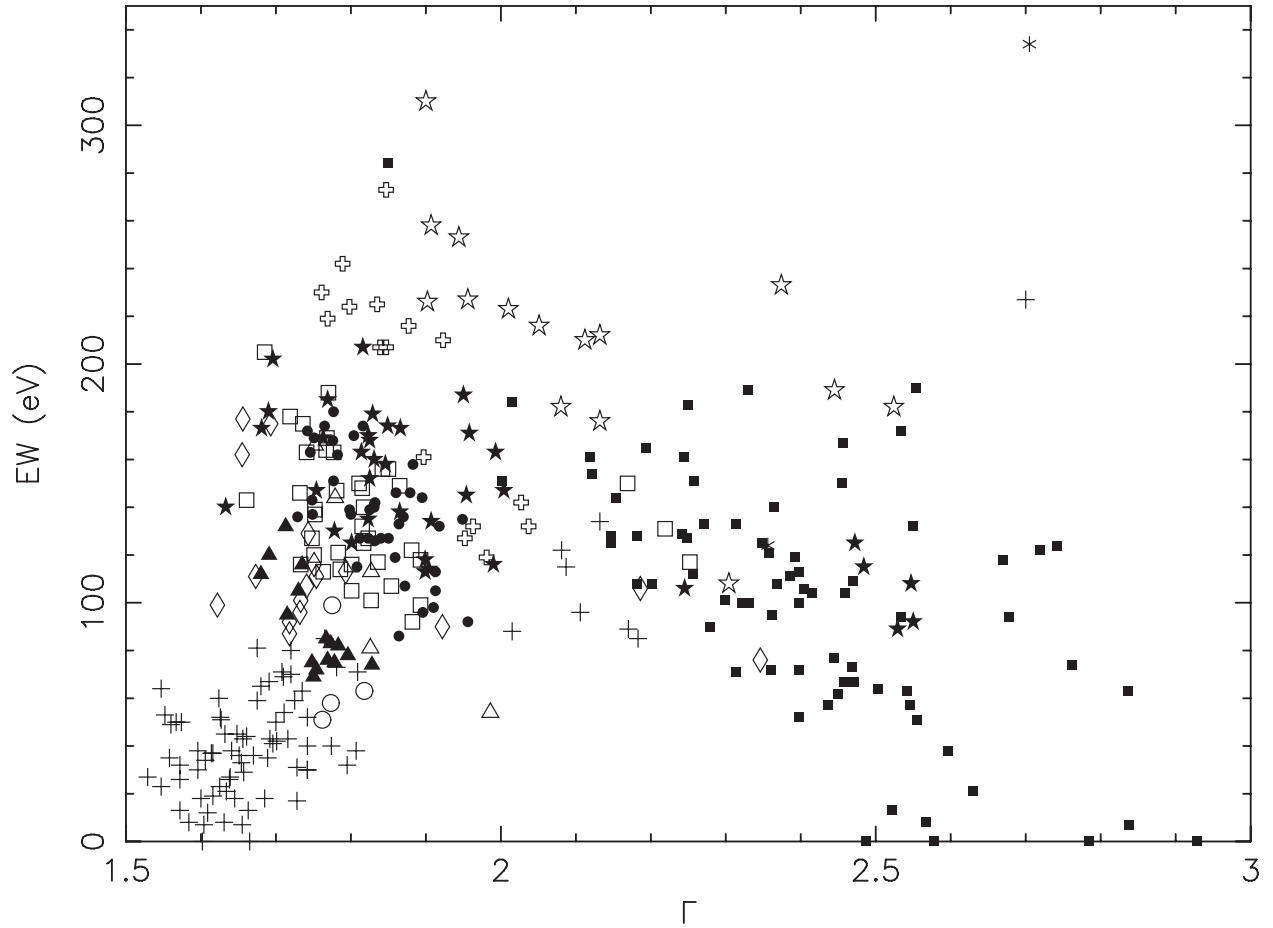


Fig. 3.— The iron line equivalent width in eV versus the powerlaw photon index. This plot is similar to the left panel in Figure 1, but with each galaxy plotted with a separate symbol. The open circles are 3C 111, open squares are 3C120, pluses (+) are 3C273, open triangles are 3C 382, open diamonds 3C 390.3, open stars Akn 120, open crosses Fairall 9, filled circles IC 4329A, filled squares MCG –6-30-15, filled triangles Mkn 509, filled stars NGC 7469, and asterisks (*) TON S180.